

# Connection between the Circumnuclear Star-Forming Regions and the active nuclei in NGC 1068

Villicaña-Pedraza I.<sup>1</sup>, <sup>\*</sup> Mast D.<sup>2</sup>, Díaz A.<sup>1</sup>, Carreto-Parra F.<sup>3</sup>, Hagele G.<sup>4</sup>, Cardaci, M.<sup>5</sup>

<sup>1</sup>*Departamento de Física Teórica, Universidad Autónoma de Madrid, Spain.*

<sup>2</sup>*Observatorio Astronómico de Córdoba, Argentina.*

<sup>3</sup>*Las Cruces, New México State University, USA.*

<sup>4</sup>*CONICET at UNLP-Universidad Nacional de La Plata.*

<sup>5</sup>*Facultad de Ciencias Astronómicas y Geofísicas, CONICET.*

8 March 2024

## ABSTRACT

In recent years, Circumnuclear Star Forming Regions (CNSFRs) have been studied in different frequencies and telescopes, diverse studies about connection between nuclear activity and star formation in the CNSFRs were doing using optical data, IFS and models. We obtain data of the Seyfert 2 galaxy NGC 1068 at J band between 1.35-1.32 $\mu$  using the 8.1m Gemini telescope and GNIRS IFU mode. We found the radial velocity and intensity maps for [FeII] $\lambda$ 12570, Pa $\beta$   $\lambda$ 12814 and FeII  $\lambda$ 13201 lines of all the components. The gas emission has a double origin associated with photoionization by young stars or excitation by collisions, we found a high influence of shocks produced by the jet. The intensity of Pa $\beta$  emission show that this component is ionized by a younger cluster or more massive stars. From the analysis of the velocity fields, the data related with the component one of Pa $\beta$  are consistent with the presence of rotation which is displaced from the maximum continuous, our observations may point to the presence of a bar.

**Key words:** Galaxies: AGN - Galaxies: Seyfert 2 - Galaxies: maps - Galaxies : NGC1068

## 1 INTRODUCTION

The Circumnuclear Star-Forming Regions (CNSFRs) with sizes until hundred of parsecs (Díaz (2000)) are constituted by several HII regions ionized by compact and bright stellar clouds. Using stellar velocity dispersions (39-67 km/s), the previous authors derived the dynamic masses for the complete stellar formation complex and the individual stellar clouds with masses from 4.9x10<sup>6</sup>Mo to 4.3x10<sup>7</sup>Mo.

There is evidence of the presence of at least two different ionized kinematic gas components in the regions. The narrow component provided by setting two Gaussian components seems to have a relatively constant value for all CNSFRs studied, with an average of 23 km/s. This narrow component could be identified with ionized gas on a rotating disc, while the stars and the gas fraction responsible for the wide component seem more related to the regions of star formation.

Furthermore, Díaz (2000) have investigated the possible connection between nuclear activity and star formation in circumnuclear galaxies CNSFRs with variable degrees of nuclear activity, concluding that there is no relationship in the formation of stars and the region of nuclear activity caused by remnants of supernovae with gas and radiation expelled from the active nucleus. Dors

(2008) combined optical IFS data (Integral Field Unit) Gemini and models to determine the abundance of gas and star forming rate on the CNSFRs of two active galaxies NGC1097 and NGC6951.

Riffel (2008) and Riffel (2010) using slicers inside GEMINI near infrared (NIFS and GNIRS in the IFU mode) studied the AGN - starburst connection and Kinematics of gas in galaxies NGC4051 active and NGC7582, respectively. They concluded that there are two forms of connection: first, molecular gas leads to the formation of stars in the circumnuclear region; second, the molecular gas is formed in the circumnuclear star formation region.

The galaxy NGC 1068 has been long considered as the prototype Seyfert 2 galaxy, but it shows wide components lines (FWHM of the order of 3500 km/s), typical emission lines of Seyfert 1 when its spectrum is obtained in polarized light AntonucciMiller (1985), Antonucci (1993) but part of the unpolarized light reaching the observer has been absorbed by the toroid. It has also been classified morphologically as a spiral galaxy of type Sab. It has angular size of 7.1' x 6'. It is located at a distance of 14.4Mpc Ulvestad (1987) and has a redshift z=0.00379 0.00001 Huchra (1999). The position of the active nuclei in far Infrared is R.A. 02 42 40.771, DEC(J2000) -00 00 47.84 Skrutskie (2006).

The mass of the black hole, derived from the observational data is about 8x10<sup>6</sup>Mo LodatoBertin (2003). Observations in wavelengths the optical-UV show that the emission is concentrated in a cone that extends to the northeast Capetti (1995), Colbert (2002).

\* E-mail: astrojupiter62@hotmail.com

The same result was detected in maps [OIII] Ruiz (2001) and [NII] Cecil (1990). The direction of polarized light cone coincides with jets observed in radio maps obtained with VLA Wilson (1982). The Cone also is seen in the southwest direction in optical-ultraviolet and [OII] but weaker. A stellar bar of 2Kpc was detected in the near infrared Scoville (1988), in turn, surrounded by a starburst circumnuclear it has also been detected in molecular gas lines Sternberg (1994) and continuous radio Gallimore (1996). The emission of this burst added to other star formation regions contribute the order half of the bolometric luminosity of the galaxy Davies (1998), JimenezBailon (2004). Optical spectroscopy made with the HST (Hubble Space Telescope) showed that NGC 1068 has a region of complex coronal lines extended to hundreds of parsecs. “The dynamics of the molecular gas in the torus show strong non-circular motions and enhanced turbulence superposed on a surprisingly slow rotation of the disk, evidence suggesting that the molecular torus is less inclined” GarciaBurillo (2016).

NGC 1068 represents an ideal object to try to establish the origin of the different kinematics components of the gas in circumnuclear regions. The aim of this work is to study the field of the velocities of the circumnuclear stellar formation regions and its possible connection with the active kernel of the galaxy. We will map field velocities of the gas in these regions with good spatial sampling, and we will separate the field velocity complexes of circumnuclear star formation, to study radial velocity of different zones to understand their effect on a possible widening of emission lines on the gas and distinguish the origin of the two components.

## 2 OBSERVATIONS AND REDUCTION

The spectroscopic data of NGC 1068 in infrared were obtained from the database of the 8.1m telescope Gemini South with GNIRS instrument in its configuration integral field spectrograph on the night of December 26, 2004. The seeing that night was between 0.6 and 0.8 arcsec in the band V. The instrument is set up in a position angle PA = 0, ie, the slices are east-west orientation.

The data analyzed in this paper were obtained with the spectrograph (GNIRS). When the Information of this work was acquired spectrograph was on the 8.1m telescope Gemini South. GNIRS provides integral field spectroscopy with a spectral resolution from  $R = (\lambda / \lambda \Delta x)$  4800 to 1600, J-band in a visual image field of  $4.8 \times 3.2$  arcsec<sup>2</sup>. The central wavelengths of the gratings GNIRS can be adjusted reaching lengths of higher or lower wavelengths. For this a network of 32 l/mm is used that depending on the angle; it can be adjusted from the X (1.10  $\mu$ m) to the M band (4.80  $\mu$ m), although generally is used in bands J, H, K (1.25  $\mu$ m to 2.20  $\mu$ m). The IFU- GNIRS divides the plane of the sky into 21 slices of 0.15 arcsec wide each. Six exposures of 300 second were conducted in the observed zone of NGC 1068. Spectra flat screen field (GCALflat) and flat field of sky were also obtained (Twilight) at exposures 2.5 sec. and 30 sec. respectively. It has also been obtained a spectrum of a calibration lamp (Arc- Lamp) with a 1.5 sec exposure to calibrate wavelength.

The reduction of these data was performed using the tasks of pack GNIRS of IRAF called GIRAF. In the process of reduction, the images were prepared to cut them (only if necessary with nscut), flat fields were created for screen and sky (nsflat), the telluric star and object of science were normalized, correction of distortion of light (nssdist), identification of the lines of the lamp was made, the sky was subtracted, the spectra obtained in the same spot were combined, the calibration was performed in wavelength

(nstransform). Finally, the 2D spectrum is extracted in a 3D cube data (nfcube). The cube contains spatial information in two directions and information Spectral on in the third. The final cube contains 651 spectra of the band J.

## 3 MEASUREMENTS AND RESULTS

### 3.1 MEASUREMENTS

The data cube contains 651 spectra obtained on J band. Each spectrum obtained has been manually analyzed component by component to keep valuable information that could help us understand in more detail the kinematics of NGC 1068. The spectrograph has 21 slices or mirrors. We obtained 31 spectra of each in order to complete the 651 mentioned. The spectra of NGC 1068 show emission lines of hydrogen recombination Pa $\beta$  ( $\lambda$ 12814) as well as [FeII]  $\lambda$ 12570 and FeII ( $\lambda$ 13201). Like the optical spectrum Arribas (1996) the emission lines in the infrared band show significant variation in their profiles with asymmetries and peaks of at least three components in many of them.

The maps were drawn from our measurement tables of the lines, creating a script that makes an order that allows IRAF to convert the information into an image that will be eventually a map. The maps are in coordinates x, y, z, where z is the value of our variable for example flux, for x, y subtends 0.15 arc seconds in the sky per pixel. The bar that accompanies each map indicates the value of each pixel by color.

Some of the spectra obtained in this work are shown (see Fig.1), note that the components of the lines are well defined, profiles so characteristic of NGC 1068. The obtained flow is in counts since they are not calibrated flow, i.e., we don't have a standard to calibrate star flow, then the y axes in our spectra is the intensity measured by not being a calibrated flow. The equivalent width (Eqw) it is the intensity of the line relative to the continuum.

In general, as shown and mentioned above, the strongest lines are Pa $\beta$  ( $\lambda$ 12814) and [FeII] $\lambda$ 12570 while FeII( $\lambda$ 13201), although it never disappears spectra, it becomes weak in most of the spectra. It is noteworthy that the Pa $\beta$  line in several spectra does not appear so could not be measured in all of them. For to analyze each line with its components has been used IRAF task splot program adjusting at least two discrete components ("d" for doublet, "g" for Gaussian fit).

### 3.2 RESULTS

In this section the results of this work show: Radial velocity of material in each region studied, flow lines and components; Intensity maps (flow) for two components of each line ([FeII]  $\lambda$ 12570 Pa $\beta$   $\lambda$  12814); FWHM maps and Eqw; Radial velocity maps; Location of the galactic nucleus on maps with coordinates of Right Ascension (RA) and Declination (DEC); understanding on behavior of the material in the study area.

The FWHM was disaffected of the instrumental width. To determine this we used the average of FWHM of the 10 most intense emission lines from the sky, obtaining a value 182 km/s. The instrumental width was quadratically subtracted to the FWHM values measured.

The line [FeII] $\lambda$ 13201 shows weak in most of the spectra, so that the mapping velocity and FWHM of that line would show a great error and it is not very reliable.

### 3.2.1 [FeII]/Pa $\beta$ Ratios .

In the map of figure 4 can be seeing the ratio of lines [FeII]/Pa $\beta$ . The ratio was made dividing the line intensities [FeII] and of Pa $\beta$  for its main component. The ratio allows separate regions where photoionization dominates. The most common values range are from 0.5 to 2. In this map (Fig. 4), the nuclear region (Marked with x) has values around 2. This would imply that there dominate the shocks, the SN, and the winds; but moving away from the region we can not say much for poor signal/noise. The map for the second component is not shown as values indicate little signal to noise.

### 3.2.2 Spectra settings on maps

Once done the maps of various line parameters of [FeII] and Pa $\beta$  it has been found the spectra configuration with respect to the maps. The maps are mapped in 21x31 arrangements (y-axis vs x axis), the scale in arcsec is 0.15x0.15 by spaxel, square. Each box on the map corresponds to a spectrum.

### 3.2.3 Error analysis

The error map gives us an idea of the regions that are acceptably measures. For the component one of the map of Pa $\beta$ , the purple regions are regions with errors smaller than 50 km/s. Blue regions, they range from 50 to 100-150 (acceptable limit). To know what is the acceptable limit according to our data, we calculated the velocity resolution and we have: if our spectrum for the line Pa $\beta$  at  $\lambda = 12800$  (approximately) has a Resolution on  $3.85(\Delta \lambda) \text{ \AA}$ , and "c" the speed of light, we use the equation  $\Delta \lambda / \lambda = \Delta V / c = 90 \text{ km/s}$  (each pixel in the spectrum). In figure 5 are error maps.

## 4 DISCUSSION

### 4.1 Intensities obtained in the Maps

The intensity maps that have been obtained in this work for lines [FeII] $\lambda 12570$  and  $\lambda 12814$  Pa $\beta$  are for main components. Riffel (2011) have worked with the Mrk 1157 galaxy observing with NIFS of Gemini telescope, making intensity maps for the same lines ([FeII] and Pa $\beta$  and its ratios, concluding that the emission flow for [FeII] increases due to shocks produced by the jet (radio), which destroys the dust grains expelling from the AGN. In addition Riffel (2011) worked with NGC 7582, which keeps recent star formation with a dark region in the central region Morris (1985); Regan (1999); Storchi (2001); Sosa Brito (2001); Wold (2006), dust is responsible for asymmetrical contours flow maps obtained while the star formation ring is circle. These clouds of star formation had not been observed in optical-IR. Comparing with the preceding information and maps obtained in this study we conclude that: i) emissions lines are elongated in the direction of the jet; ii) the emission of flow for [FeII] in both components is greater than for Pa $\beta$  components, which means influence of shocks produced by the jet; iii) More intensity in the emission of Pa $\beta$  for component 1 would imply a ionization region of the component 1 due to a younger cluster, or where there are more massive stars that ionize the gas.

### 4.2 FWHM from maps

Riffel (2010) studied NGC 7582, reporting the presence of a broad component of Bry line with FWHM of 4000 km/s. Another broad

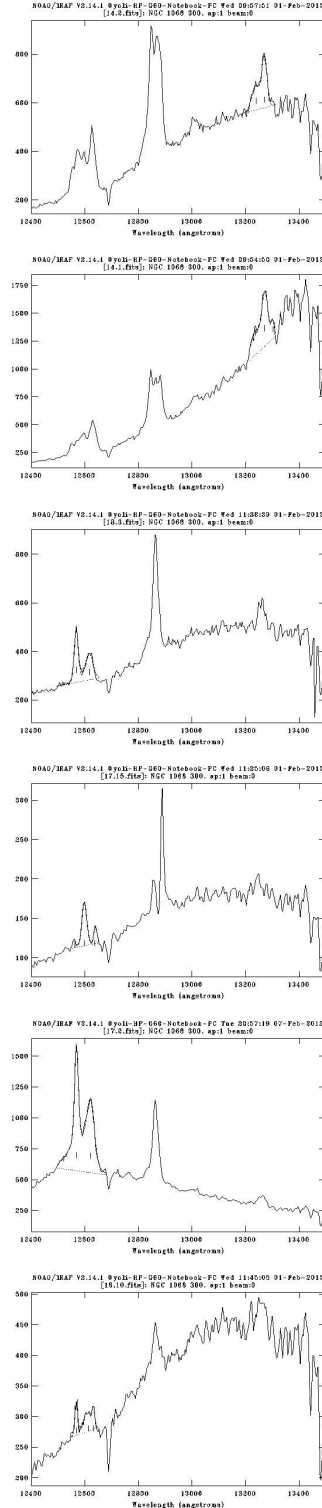


**Figure 1.** Most representative spectra obtained 651 spectra which can be seen clearly three lines of emission on that have been analyzed. El spectral range for the X axis ( $\lambda$ ) is 12000-13000  $\text{\AA}$ . The Y axis is in accounts (intensity)

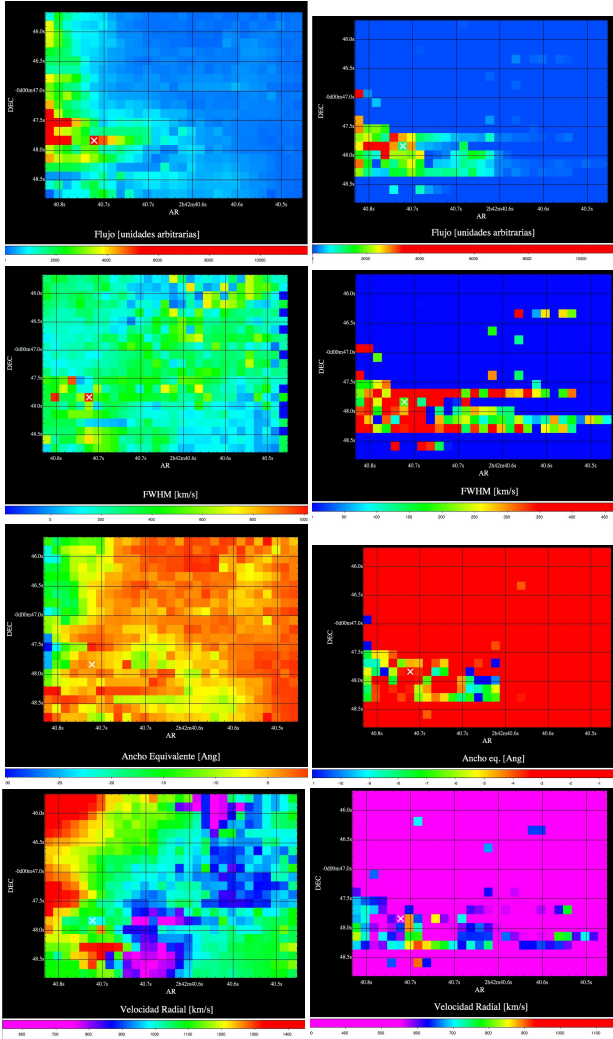


**Figure 2.** Flux maps for FeII line  $\lambda 12570$  (one for two images); first block at center: FWHM maps in km/s; Centering second block, Eqw  $\text{\AA}$ ; Finally, radial velocity maps in km/s. Color bar indicate parameter value. Left maps are for the first component, while, right maps to the second. Maps orientation is North up, east left. There are not maps for the third component because low signal to noise and was detected in a reduced region of the field.

component observed (which disappeared) is  $h\alpha$  and had also been reported by [Aretxaga \(1999\)](#), the latter seemed to have been caused by a transient event and proposed three possible scenarios for its origin: i) Capture and breaking of a star by a supermassive black hole. ii) A change in the redness of the toroid surrounding the core. iii) An explosion of Supernova Type II.

In this paper the map of FWHM for [FeII] has values ranging from 200-800 km/s being the most dominant about 600 km/s, indicating increased gas turbulence in the area where that line is produced causing wider and deformed lines by turbulence.

From the maps obtained in this work, we found that for  $\text{Pa}\beta$  line the FWHM obtained for component one is higher than for the component two with values ranging from 100-500 km/s and 100-300 km/s respectively with maximums at 300 km/s and 100 km/s respectively. We conclude that there exists more gas turbulence in this line for component 1 than in component 2.

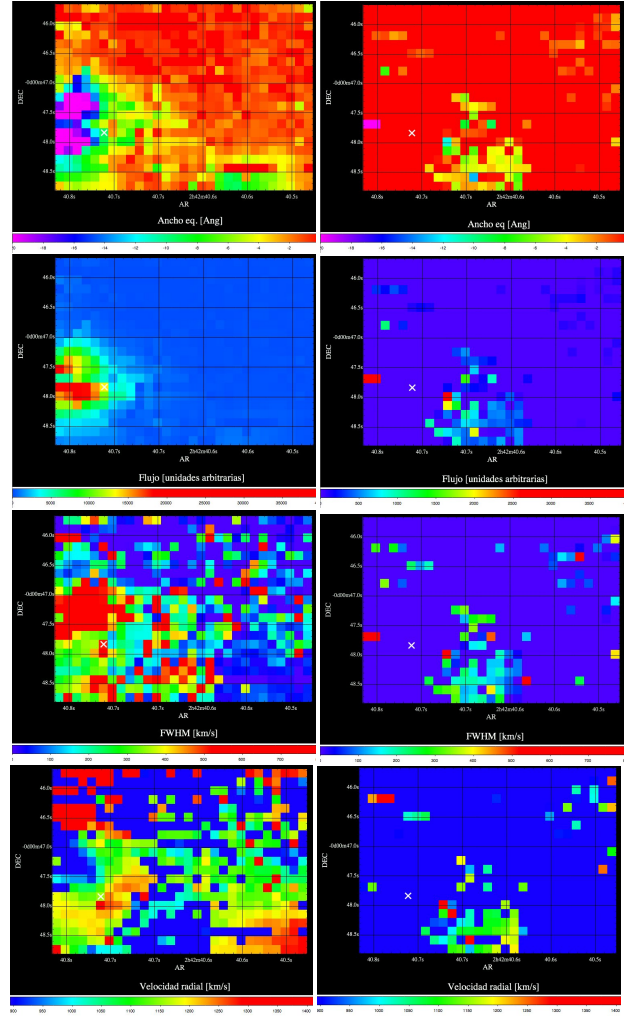


**Figure 3.** Up: EqW maps of the  $\text{Pa}\beta 12814$  line in  $\text{\AA}$ ; First block at the center, flux maps; Second block at the center, FWHM maps in km/s. Last one, Radial velocity maps in km/s. Color bar indicate parameter value. Left maps are for the first component, while, right maps to the second. Maps orientation is North up, east left. There are not maps for the third component because low signal to noise

### 4.3 EqW from Maps

In his study of NGC 7582 [Riffel \(2010\)](#) found for Bry line an Eqw of  $30\text{\AA}$  and stellar formation of 5Myr. [Dors \(2008\)](#) found similar values of CNSFRs in NGC6951 and NGC1097. A greater Eqw indicate more star formation as shown [Rodriguez \(2010\)](#). For this paper, we can see that, in the case of the Eqw of [FeII] $\lambda 12570$ , we have values from  $3\text{-}30\text{\AA}^{-1}$ . In the component one centered at  $3\text{\AA}$ , and for the component two, values are similar. While in the case of Eqw of  $\text{Pa}\beta$  for component one, it has values from  $1\text{-}6\text{\AA}$  and for the component two, it has values dominated for  $1\text{-}2\text{\AA}$ .

Because the component 1 shows an EqW of  $\text{Pa}\beta$  bigger, we can estimate that this component would occur in an area with more recent star formation or abundant.

### 4.4 Ratio lines

The map obtained can observe the ratio of the lines [FeII]/ $\text{Pa}\beta$ . The ratio allows separating regions where photoionization and shock regions dominate. The most common values are 0.5 to 2. In this map

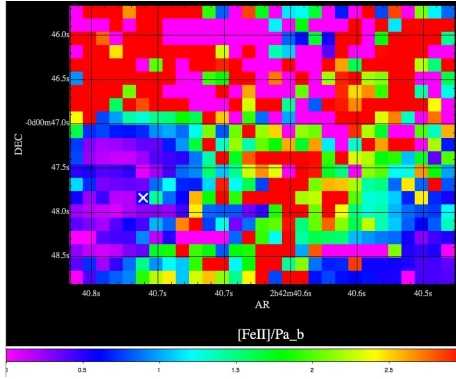


**Figure 4.** Ratio map of Intensity of FeII/Pa $\beta$  using the principal component of each line respectively. Orientation of the map is North up and east left.

the nuclear region (marked with x) has values around 2. This implies that there dominate the shocks, the SN, and the winds; but moving away from the region we can not say much because poor signal/noise. The map for the second component is not shown because the values indicate little signal to noise and higher errors.

#### 4.5 Radial velocity and dispersion velocity

The optical spectra of the nuclear region show clear signs of middle-aged stars (Cid-Fernandes (2002)). About the kinematics of gas, the blue shift could be due to an inflow if the gas is located in the plane or a outflow if the gas is extended at high latitudes above the plane (conical structure facing us). Riffel (2010) studied NGC 7582, the radial velocity field shows a blue shift toward SE and a redshift NW, suggesting rotation although the kinematic center is shifted from the continuous emission peak. They concluded that the stellar velocity field shows distorted rotation which is offset relative to the core 50 pc (continuous peak); The distortion may be due to a bar in the nucleus. In this work the velocity for the two components are of 1200 km/ and 600 km/s for the line [FeII], while for the line Pa $\beta$  we have 1150 km/s and 700 km/s. In the work of Mazzalay (2010) NGC 1068 was studied (with NIFS at 1.15-1.3 microns) but it was not adjust each of the lines of interest manually, it built codes to analyze them losing valuable kinematics information from different components. Riffel (2010) studied NGC 1066 with NIFS (1.10-1.35 microns) to obtain a very similar to that presented in this paper (GNIRS), but adjustments the same lines without considering the components, losing kinematics information of the galaxy.

## 5 CONCLUSIONS

In this paper, 651 spectra were obtained from NGC1068 between 1.25-1.32 microns , in these spectra have being identified the most important emission lines [FeII] $\lambda$ 12570, Pa $\beta$   $\lambda$ 12814 and FeII  $\lambda$ 13201.

For each of the lines, it has made an adjustment of multicomponent obtaining up to five components to the same line in some spectra, which in this work only the two most important were presented and mapped: [FeII] $\lambda$ 12570 , Pa $\beta$   $\lambda$ 12814 being obtained the velocity field.

The information obtained for the observed distribution of flow in the two mapped components has shown that the emission gas in each has a double origin. It has being associated with photoionization by young stars, or excitation by collisions. The nuclear emis-

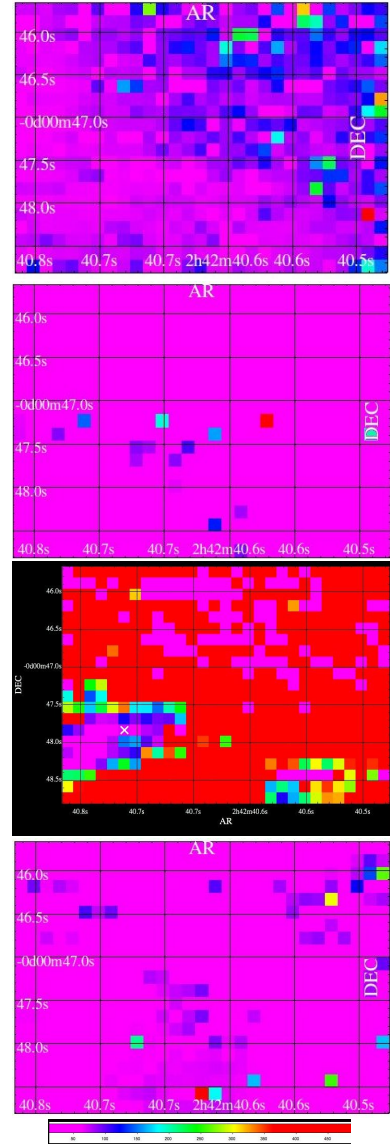


**Figure 5.** Error maps for radial velocity. On the Superior part are the error maps for [FeII]. Inferior part, the corresponding maps to the Pa $\beta$  line. The maps are show for two components, the first at left, and second at right. The color bar represents the error value km/s. To get error maps we use the Keel formula (1996).

sion for [FeII] in both components is greater than Pa $\beta$ , which means a high influence of shocks produced by the jet; Moreover, the emission intensity of the Pa $\beta$  line is high for the component 1, which imply that this component is ionized by a younger cluster, or there are more massive stars. The Map FWHM for [FeII] has higher values for component 1, indicating greater gas turbulence in the zone where the line is measured causing deformed wider lines by turbulence. For Pa $\beta$  line, the FWHM obtained for component 1 is greater than for the component 2. We conclude that for this line, there is greater gas turbulence shown in componte 1 than component 2.

We Obtained for the case of eqw of [FeII] $\lambda$ 12570 similar data values for the two components show slightly lower in the component 2; For the component two of the Pa $\beta$  line, values shown slightly lower than for the component 1. Because the component 1 shows a greater Eqw of Pa $\beta$  we can estimate that it would occur in

an area with more recent star formation or abundant. On the map shown, marked with x, the nuclear region has values around 2. This would imply that the shocks, the SN, and the winds dominate there; but moving away from this area, we can not say much due to poor signal to noise and greater errors. The map for the second component is not shown because values indicate very low signal to noise ratio and increased errors.

Finally, from the analysis of the velocity field is obtained that the component one of [FeII] line is for greater than component 2. In the same way, the velocity is higher in component one than component two for Pa $\beta$  line. The data relating to the component 1 are consistent with the presence of rotation. However, it is hard to distinguish this effect produced by a jet. In the event that the rotation is displaced from the maximum continuous, our observations may point to the presence of a bar.

#### ACKNOWLEDGEMENTS

This work has been supported by the Universidad Autonoma de Madrid fellowship 2010-2011. A special gratitude to Luc Binette from UNAM for the support in my short stay with him. My special gratitude to German Gimeno from Gemini Telescope for the amazing experience at the telescope. A special appreciation to Antonio Sanchez Ibarra, Carmen Mendiola, Hector P. Coiffier, Rocio P. Mendiola, K. Paola Tellez (and Pity). My gratitude to Luis Felipe Rodriguez from IRYA, Sergio Martin from ESO, Damian Mast from the Observatorio Astronomico de Cordoba, Angeles Diaz from Universidad Autonoma de Madrid, and Rolf Guesten from Max Planck for Radioastronomy for believing in me.

#### REFERENCES

- Antonucci, R., 1993, ARAA, 31, 473.  
 Antonucci, R. and Miller, J., 1985, ApJ, 297, 621.  
 Aretxaga, I. et al., 1999, ApJL, 519, L123.  
 Arribas, S. et al., 1996, ApJ, 463, 509.  
 Capetti, A. et al., 1995, ApJL, 452, L87.  
 Cecil, G. et al., 1990, ApJ, 355, 70.  
 Colbert, E. et al., 2002, ApJ, 581, 182.  
 Davies, R. et al., 1998, MNRAS, 300, 388.  
 Díaz, A. et al., 2000, MNRAS, 311, 120.  
 Dors, J.O. et al., 2008, AAP, 482, 59.  
 Emsellem, E. et al., 2006, MNRAS, 365, 384.  
 Exposito, J. et al., 2011, AAP, 533, A63.  
 Fanaroff, B. and Riley, J., 1974, MNRAS, 167, 31P.  
 Gallimore, J. et al., 1996, AAS, 1421, 28.  
 Garcia Burillo, S. et al., 2016, ApJL, 823, L12.  
 Hagele, G. et al., 2010a, MNRAS, 406, 1675.  
 Hagele, G. et al., 2010b, MNRAS, 402, 1005.  
 Hagele, G. et al., 2009, APSS, 324, 341.  
 Hagele, G. et al., 2007, MNRAS, 378, 163.  
 Heckman, T., 1980, AAP, 87, 152.  
 Huchra, J. et al., 1999, VizieR Online Data Catalog, 212, 10287.  
 Jimenez Bailon, E., 2004, Thesis.  
 Lodato, G. and Bertin, G., 2003, AAP, 398, 517.  
 Mazzalay, X., 2010, Thesis.  
 Morris, S. et al., 1985, MNRAS, 216, 193.  
 Osterbrock, D. and Martel, A., 1993, ApJ, 414, 552.  
 Osterbrock, D.E., 1989, book, 1.  
 Rafanelli, P. et al., 2011, Baltic Astronomy, 20, 419.  
 Regan, M. and Mulchaey, J., 1999, AJ, 117, 2676.  
 Riffel, R. et al., 2011, MNRAS, 411, 469.  
 Riffel, R. et al., 2010, MNRAS, 404, 166.  
 Riffel, R. et al., 2008, MNRAS, 385, 1122.  
 Rodriguez-Ardilla, A. et al., 2011, ApJ, 743, 100.  
 Rodriguez-Zaurin, J. et al., 2010, MNRAS, 403, 1317.  
 Ruiz, J. et al., 2001, AJ, 122, 2961.  
 Scoville, N. et al., 1988, ApJL, 327, L61.  
 Simpson, J. et al., 2002, ApJ, 574, 95.  
 Skrutskie, M. et al., 2006, AJ, 131, 1163.  
 Sosa-Brito, R. et al., 2001, ApJS, 136, 61.  
 Sternberg, A. et al., 1994, ApJL, 436, L131.  
 Storchi-Bergmann, T. et al., 2001, ApJ, 559, 147.  
 Ulrich, M. et al., 1997, ARAA, 35, 445.  
 Ulvestad, J. et al., 1987, AJ, 93, 22.  
 Urry, C. and Padovani, P. et al., 1995, PASP, 107, 803.  
 Villicana-Pedraza, I., 2010, Thesis.  
 Wilson, A. and Ulvestad, J., 1982, ApJ, 263, 576.  
 Wold, M. and Galliano, E., 2006, MNRAS, 369, L47.

This paper has been typeset from a  $\text{\TeX}/\text{\LaTeX}$  file prepared by the author.